

https://doi.org/10.1070/QEL17665

All-glass single-mode microstructured optical fibres with a large-diameter core and low bending losses

A.N. Denisov, S.L. Semjonov

Abstract. **All-glass microstructured optical fibres (MOFs) with a core 20 μm in diameter and two rings of circular fluorine-doped silica glass elements with a reduced refractive index, different diameters, and different distances between them are theoretically studied. The properties of these MOFs are numerically analysed using the finite element method. The leakage losses for the fundamental and higher-order modes in the spectral range 0.75–1.65 μm are calculated for straight and bent MOFs. It is shown that the considered MOF design allows single-mode operation in the range 0.98–1.26 μm at a bending radius of down to 0.08 m, the leakage losses for the bent MOF at a wavelength of 1.05 μm being 0.046 dB m^{-1}.**

Keywords: *microstructured optical fibres, single-mode optical fibres, large mode area fibres, finite element method.*

1. Introduction

Single-mode optical fibres with a large mode area belong to the main elements of high-power fibre lasers and amplifiers, which are used in many fields, including processing of industrial materials, fundamental sciences, and medicine [1–5]. Similar properties are typical of various types of microstructured optical fibres (MOFs), such as photonic bandgap fibres [6–13], Bragg fibres [14–17], and leakage channel fibres (LCFs) [18–22]. The use of leakage channels is one of rather simple methods of forming single-mode MOFs with a large-diameter core and, hence, a large mode area by selecting hole diameters d and distances between them Λ that ensure low leakage losses for the fundamental mode (below 0.1 dB m^{-1}) and simultaneously high leakage losses for higher-order modes (exceeding 1.0 dB m^{-1}) [18]. However, the MOF designs with air holes have some drawbacks related both to complicated fabrication of MOF structures with required parameters, especially if it is necessary to have holes with different diameters, and to the problems of their fusion with conventional fibres due to collapse of holes, which leads to additional losses.

These drawbacks can be eliminated using all-glass MOFs with a cladding formed by elements of fluorine-doped silica glass with a reduced refractive index [23–27]. But the range of characteristics of these MOFs, both theoretically studied and fabricated to date, is limited due to the hexagonal configuration of their elements, which implied the use of the method for assembling preforms of MOFs of rods with different compositions. In particular, bending losses for MOFs in [23] with a bending radius of 0.2 m exceeded 30 dB m^{-1}. The authors of [24] succeeded to achieve bending losses of about 0.5 dB m^{-1} for LCF7 at a bending radius of 0.15 m but only in the case of bending in one direction, while these losses in the case of bending in the other direction were an order of magnitude higher (about 5 dB m^{-1}). Since, in practice, the orientation of the MOF internal structure with respect to the bending direction cannot be strictly controlled, these MOFs are not of much practical interest.

A considerably wider variety of the structural parameters of MOFs and, therefore, of their physical characteristics, is provided by the method consisting in the drilling of holes in a pure silica rod, subsequent insertion of fluorine-doped silica rods in these holes, and extrusion of this preform into a MOF with required parameters.

A.N. Denisov, S.L. Semjonov Prokhorov General Physics Institute of the Russian Academy of Sciences, Dianov Fiber Optics Research Center, ul. Vavilova 38, 119333 Moscow, Russia;
e-mail: denisov@fo.gpi.ru

Received 26 October 2021
Kvantovaya Elektronika **51** (12) 1081–1089 (2021)
Translated by M.N. Basieva

2. Geometric structure of MOFs

In the present work, we theoretically study an original design of an all-glass MOF that was previously proposed and partially theoretically investigated by us in [28]. This MOF has a large pure silica glass core surrounded by two rings of circular elements with different diameters and distances between them, which are made of fluorine-doped silica glass with a reduced refractive index (Fig. 1).

The MOF core represented by the dashed circle has diameter D_{core}. The first ring contains six identical elements with diameter d_1 and distance Λ_1 between them. Twelve elements of the second layer have different diameters, namely, $d_2 > d_1$ and $d_3 \leqslant d_2$; the elements with diameters d_2 are positioned opposite the spaces between the elements of the first ring and at distance Λ_2 from these elements, while elements with diameters d_3 are located opposite the elements of the first ring at distance Λ_3 from them. This variant is conventionally called MOF-18, where 18 is the total number of elements.

This algorithm of constructing the MOF-18 structure extends the possibilities of varying its parameters in order to optimize the MOF characteristics, in particular, leakage losses for the fundamental and higher-order modes. The optimal relation between the MOF-18 parameters for a particular problem can be determined using the multi-objective optimisation algorithm, but this may take several days of continuous calculations even with the use of a supercomputer [29]. Because of this, we chose a relatively simple problem, namely, we tried to achieve single-mode operation in the spectral region near $\lambda = 1.05$ μm for a MOF-18 with the core diameter

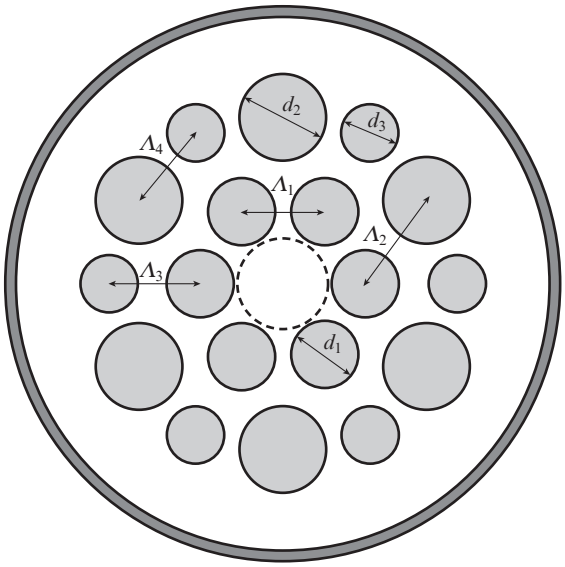

Figure 1. Transverse structure of MOF-18: $d_1/\Lambda_1 = 0.82$, $d_2/d_1 = 1.25$, $d_3/d_1 = 0.90$, $\Lambda_2/\Lambda_1 = 1.25$, and $\Lambda_3/\Lambda_1 = 1.10$.

$D_{core} = 20$ μm at a fixed relation between the diameters of elements, that is, at $d_2/d_1 = 1.15$ and $d_3 = d_1$. The other parameters of the MOF-18 structure were determined by trial and error with the purpose to obtain admissible leakage losses for the fundamental and higher-order modes at some chosen control wavelengths. In addition, since, in practice, a part of the optical fibre length can be straight and the other part can be bent, the appropriate structural parameters were sought taking into account losses for both straight and bent MOF-18.

In [28], we performed calculations for a MOF-18 with fluorinated silica glass elements whose refractive index was lower than that of pure silica glass by $\Delta n \sim 1.5 \times 10^{-3}$ and obtained single-mode operation in the spectral region near 1.05 μm only at a bending radius down to 0.25 m. In the present work, we chose $\Delta n = 4 \times 10^{-3}$ and tried to find the MOF-18 structure parameters that ensured single-mode operation near 1.05 μm at a bending radius down to 0.08 m. The choice of this aim is explained by the existence of widespread optical fibre coils 0.16 m in diameter, which make it possible to design rather compact devices (for example, fibre lasers and amplifiers). We also considered in detail the MOF-18 characteristics for better understanding of its properties and possibilities of further improvement of its parameters for solving particular practical problems.

3. Calculation results

The MOF-18 characteristics were numerically calculated using the finite element method (FEM) with a cylindrical perfectly matched layer (PML), whose parameters provide a necessary accuracy of determination of leakage losses in the case of a limited size of the model structure. From the physical point of view, the PML can be considered as a layer with almost ideal absorption. The PML in Fig. 1 is shown by a dark-grey ring.

As a material for the MOF-18, we used silica glass with refractive index n_{sil}, which was determined with the use of the Sellmeier equation [30].

3.1. Straight MOF-18

Figure 2 shows the spatial intensity distributions for two polarisations (denoted by red arrows) of the fundamental mode (1 and 2) and four higher-order modes (denoted by figures from 3 to 6 in descending order of the real part of their effective refractive index n_{eff}) at a wavelength of 0.9 μm for a straight MOF-18 with the following chosen parameters: $d_1/\Lambda_1 = 0.795$, $\Lambda_2/\Lambda_1 = 1.226$, and $\Lambda_3/\Lambda_1 = 1.103$. Note that these parameters differ from the MOF-18 parameters given in Fig. 1, which are used only for illustration.

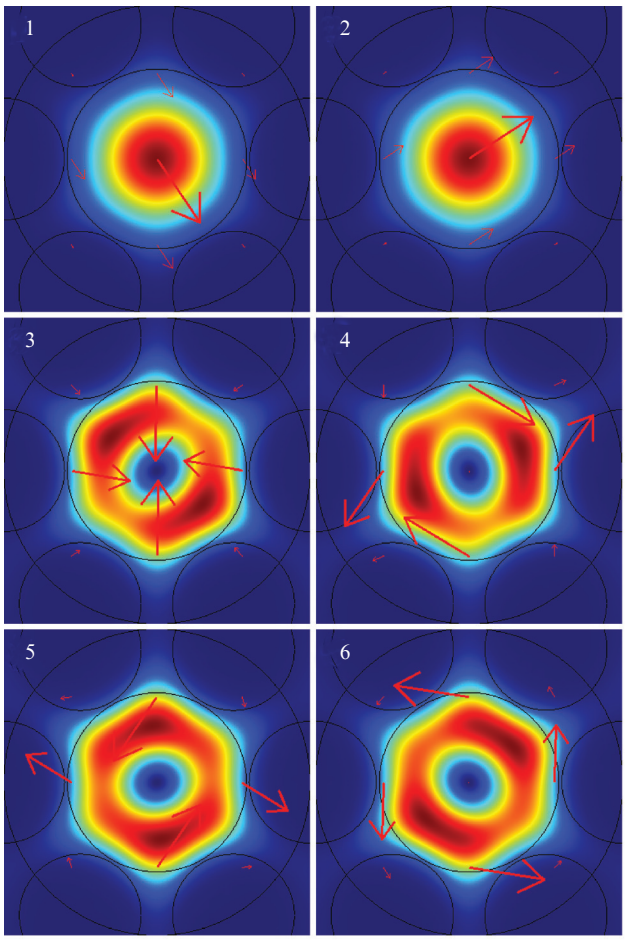

Figure 2. (Colour online) Spatial intensity distributions of (1, 2) fundamental and (3–6) higher-order modes of a straight MOF-18 at $d_1/\Lambda_1 = 0.795$, $d_2/d_1 = 1.15$, $d_3/d_1 = 1.0$, $\Lambda_2/\Lambda_1 = 1.226$, and $\Lambda_3/\Lambda_1 = 1.103$ for a wavelength of 0.900 μm.

Modes 1 and 2 belong to the HE_{11} type and differ only in polarisation; mode 3 is the TM_{01} mode, 4 and 5 are the HE_{21} modes, and 6 is the TE_{01} mode [31]. Leakage losses α (in dB m^{-1}) were determined from the calculated imaginary part of refractive index k_{eff} by the formula [32]

$$\alpha = \frac{20}{\ln 10}\frac{2\pi}{\lambda}k_{eff}. \quad (1)$$

Figure 3 presents the spectral dependences of leakage losses for the fundamental and higher-order modes of the MOF-18 in the range of 0.75–1.65 μm and designates loss

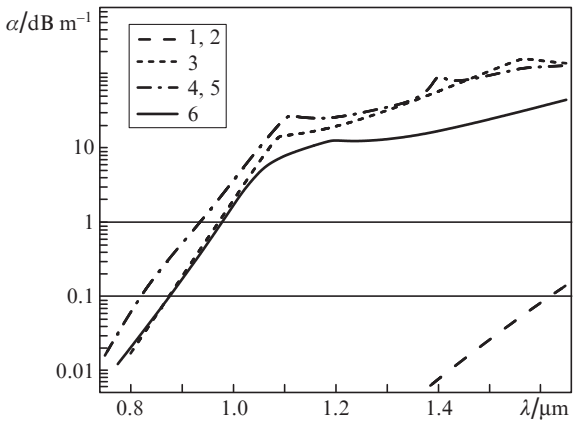

Figure 3. Spectral dependences of leakage losses in a straight MOF-18 for (1, 2) fundamental and (3–6) higher-order modes.

levels of 0.1 and 1.0 dB m^{-1}, which allow one to determine the edges of the single-mode range [18]. One can see that the spectral range of the single-mode regime for the straight MOF-18 is 0.98–1.62 μm.

It should be noted that, at wavelengths longer than ~0.9 μm, a noticeable part of the intensity of modes 3–6 is located between the rings of elements (for convenience, we will call this region the annular space). In this case, one observes additional modes, which have the same spatial intensity distributions in the MOF-18 core as corresponding modes 3–6 but different ratios of intensities in the core and the annular space, as well as different levels of leakage losses. In addition, these modes slightly differ in the real part of refractive index n_{eff}, because of which we will denote them as Ma, Mb, Mc, and so on (where M is the mode number from 3 to 6) in descending order of their n_{eff}. Since the most important part of our problem (finding of the spectral range of the single-mode regime of MOF-18) is to determine the minimal losses for higher-order modes, then, for the spectral dependences shown in Fig. 3, we naturally selected from several modes Mi only one mode that had lowest leakage losses for a particular wavelength (for each number M). Note that, in the studied spectral range, the modes with numbers Mc (and further) have considerably higher losses than modes Ma and Mb, because of which they are not considered.

To illustrate the aforesaid, Fig. 4 shows the spatial intensity distributions of modes 3a and 3b for wavelengths of 0.900, 1.050, 1.089, and 1.567 μm, and Fig. 5 presents the spectral dependences of leakage losses for these modes. One can see that, almost in the entire studied wavelength range, modes 3a and 3b are localised in both the core and the annular space (cladding), that is, strictly speaking, these modes are not purely core modes and must be generally considered as higher-order modes of MOF-18.

As follows from Fig. 4, the main difference between modes 3a and 3b consists in the orientation of the electric field vector in the annular space, that is, this vector for mode 3a is directed radially either from or to the MOF-18 core identically with the electric field vector of this mode in the MOF-18 core, while the electric field vectors in the core and annular space for mode 3b are directed in opposite directions. The resultant spectral dependence of leakage losses for mode 3, which is shown in Fig. 3, corresponds to the minimum values among the losses for modes 3a and 3b presented in Fig. 5. This explains the noticeable bends in the resultant spectral dependence of leakage losses for mode 3 (see Fig. 3) at wavelengths of 1.089 and 1.567 μm, where the losses for modes 3a and 3b become equal.

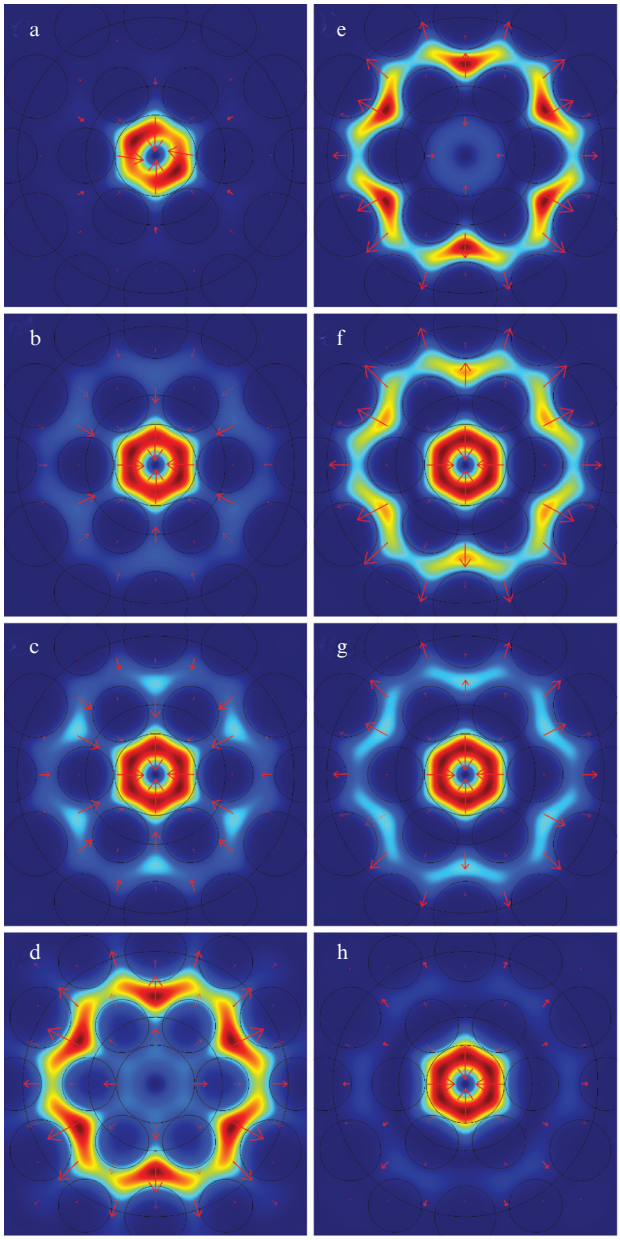

Figure 4. (Colour online) Spatial intensity distributions of modes (a–d) 3a and (e–h) 3b in a straight MOF-18 for wavelengths of (a, e) 0.900, (b, f) 1.050, (c, g) 1.089, and (d, h) 1.567 μm.

The situation for modes 4, 5, and 6 is in general similar, that is, for these modes one also observes two similar in spatial intensity distributions in the MOF-18 core modes 4a and 4b, 5a and 5b, and 6a and 6b. However, the spatial intensity distributions of these modes in the annular space have a specific azimuthal character different from that for modes 3a and 3b. In this case, similar to modes 3a and 3b, the main difference between modes Ma and Mb (M = 4–6) consists in different orientations of electric field vectors in the annular space. Thus, we can conclude that the higher-order modes of MOF-18 have twofold degeneracy caused by the presence of additional different intensity maxima in the annular space for these modes.

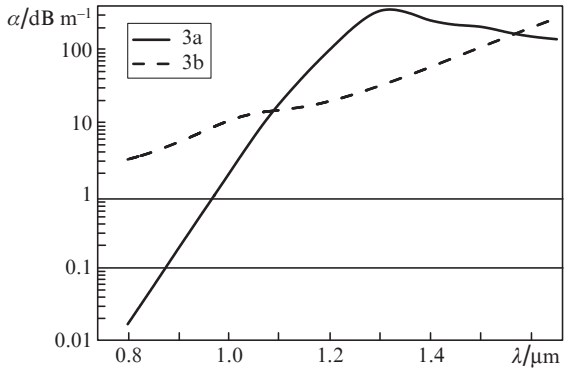

Figure 5. Spectral dependences of leakage losses in a straight MOF-18 for modes 3a and 3b.

3.2. Bent MOF-18

The leakage losses for bent MOF-18 were calculated by replacing it with a straight fibre having an equivalent refractive index n_{equ} determined (in the case of bending in the x axis direction) using the expression [33]

$$n_{equ}(x,y) = n(x,y)\left(1 + \frac{x}{R}\right), \qquad (2)$$

where $n(x,y)$ is the initial refractive index profile of straight MOF-18 and R is the bending radius in meters. A similar equation but with replacement of x for y in (2) was used to calculate the leakage losses in MOF-18 bent in the y axis direction.

Figure 6a shows the spatial intensity distributions for two polarisations of the fundamental mode (1 and 2) and four higher-order modes (from 3 to 6 in the descending order of their n_{eff}) at a wavelength of 0.9 μm for a MOF-18 bent in the x axis direction with the bending radius $R_x = 0.08$ m. Modes 3 and 4 belong to the LP_{11o} type and differ only in polarisation, while modes 5 and 6 are LP_{11e} modes and also differ only in polarisation [34].

For comparison, Fig. 6b presents the corresponding distributions for a MOF-18 bent in the y axis direction with bending radius $R_y = 0.08$ m. Since, as is seen from comparison of Figs 6a and 6b, the images of higher-order modes only slightly differ with bending in the y direction, they are denoted analogously to the higher-order modes in the case of bending in the x direction, although the real parts of their refractive indices n_{eff} vary differently. The denotation of fundamental modes 1 and 2 was chosen in the descending order of the absolute value of the imaginary part of their effective refractive index k_{eff}, that is, in the descending order of their leakage losses. This choice provides a bottom estimate of the spectral range of single-mode regime when using fundamental mode 1, which ensures a certain reliability of determined values.

Figure 7 shows the spectral dependences of leakage losses for the fundamental and higher-order modes of MOF-18 bent in the directions of the x (Fig. 7a) and y (Fig. 7b) axes. One can see that the spectral range of a single-mode regime for bent MOF-18 is 0.93–1.11 μm in the case of bending in the x direction and 0.94–1.12 μm in the case of bending in the y direction, that is, the spectral ranges almost coincide. One can also note that the leakage losses for fundamental mode 1 at a wavelength of 1.05 μm are almost identical for bends in different directions, namely, they are 0.049 dB m^{-1} for $R_x = 0.08$ m and 0.048 dB m^{-1} for $R_y = 0.08$ m.

A considerable part of the intensity distribution of modes 3–6 in the bent MOF-18 (as well as in the straight one) is located in the annular space. In this case, there exist additional modes, which have the same spatial intensity distributions in the MOF-18 core as the corresponding modes 3–6 but differ in the intensity ratios in the core and in the annular space, as well as in the leakage loss levels. In addition, they have somewhat different real parts of effective index n_{eff}, because of which we will again denote these modes as Ma, Mb, Mc, and so on (M is the mode number from 3 to 6) in the descending order of their n_{eff}. Similar to the above case with the straight MOF-18, to obtain the spectral dependences shown in Fig. 7, we selected from several modes Mi only one mode that had the lowest leakage loss for a particular wavelength (for each M).

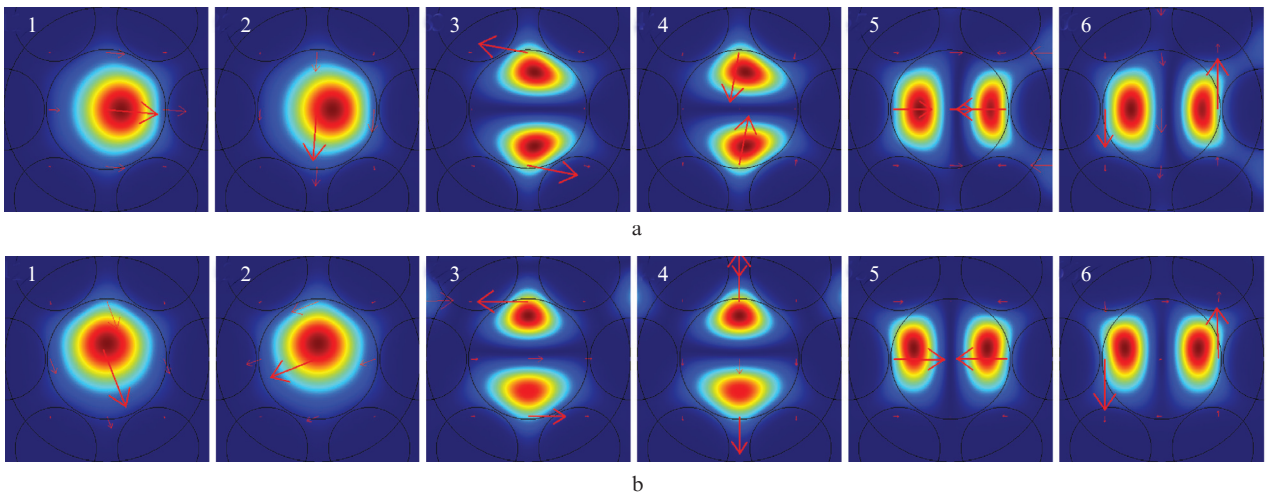

Figure 6. (Colour online) Spatial intensity distributions of (1, 2) fundamental and (3–6) higher-order modes in bent MOF-18 for a wavelength of 0.900 μm at (a) $R_x = 0.08$ m and (b) $R_y = 0.08$ m.

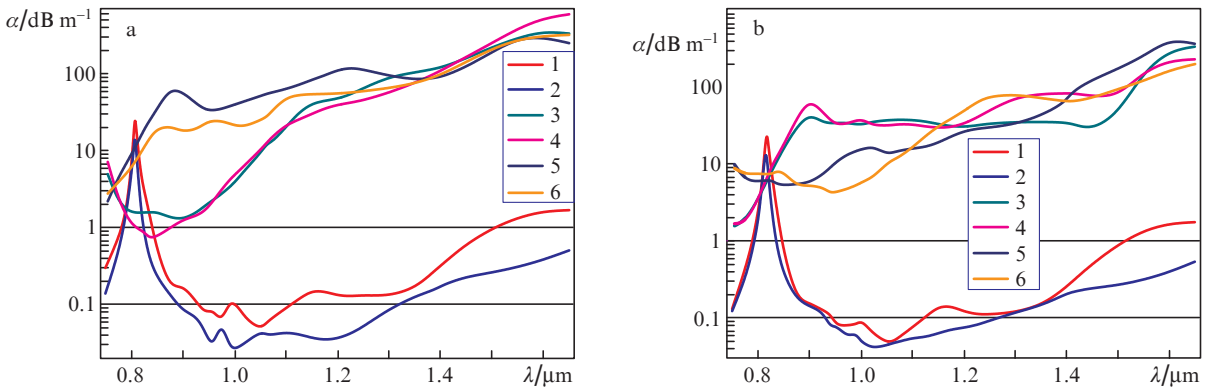

Figure 7. (Colour online) Spectral dependences of leakage losses in bent MOF-18 for (1–6) fundamental and higher-order modes at (a) $R_x = 0.08$ m and (b) $R_y = 0.08$ m.

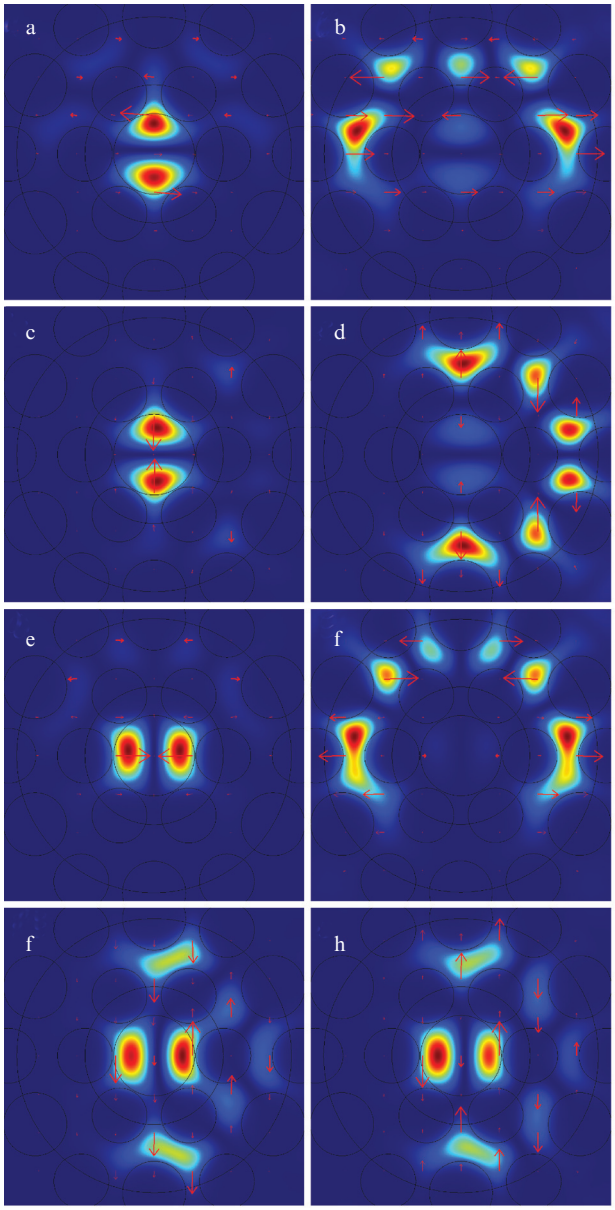

Figure 8. (Colour online) Spatial intensity distributions of higher-order modes in bent MOF-18 at a wavelength of 1.175 μm for modes (a) 3a and (b) 3b at $R_y = 0.08$ m, (c) 4a and (d) 4b at $R_x = 0.08$ m, (e) 5a and (f) 5b at $R_y = 0.08$ m, and (g) 6a and (h) 6b at $R_x = 0.08$ m.

The aforesaid is illustrated in Fig. 8, which presents the spatial intensity distributions of mode pairs Ma and Mb (M = 3–6) of bent MOF-18 for a wavelength of 1.175 μm at $R_x = R_y = 0.08$ m. Figure 9 shows the spectral dependences of leakage losses for modes 5a and 5b at $R_x = 0.08$ m. The resultant spectral dependence of leakage losses for mode 5 (see Fig. 7a) represents the minimum among the two curves for modes 5a and 5b given in Fig. 9. Thus, the higher-order modes in MOF-18 bent in different directions are also at least doubly degenerate because they have additional different intensity maxima in the annular space.

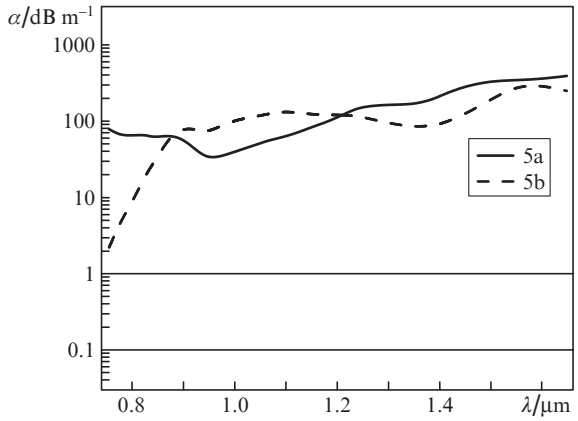

Figure 9. Spectral dependences of leakage losses in a bent MOF-18 at $R_x = 0.08$ m for modes 5a and 5b.

4. Discussion of results

Returning to Fig. 7, note pronounced maxima in the spectral dependences of leakage losses for fundamental modes 1 and 2 near a wavelength of 0.8 μm. Although they lie rather far from the spectral region of interest (1.05 μm), it is necessary to clearly understand the mechanism of their appearance to take them into account and correct the MOF-18 parameters when solving other problems. Despite the fact that the shapes of these maxima resemble some resonance dependences, in reality, this behaviour of losses is due to the presence of modes 1a and 1b, as well as 2a and 2b, near this wavelength, which have similar spatial intensity distribu-

tions in the MOF-18 core but simultaneously have additional intensity maxima in the annular space, that is, in the cladding.

This is illustrated in Fig. 10, which shows the spatial intensity distributions of modes 1a and 1b of a MOF-18 bent with $R_x = 0.08$ m at wavelengths of 0.8050, 0.8075, and 0.8150 μm. One can see that the main difference between the additional maxima for modes 1a and 1b consists in the orientation of the electric field vector, that is, this vector for mode 1a in the annular space is directed similarly to this vector in the MOF-18 core, while the corresponding vectors for mode 1b are directed oppositely.

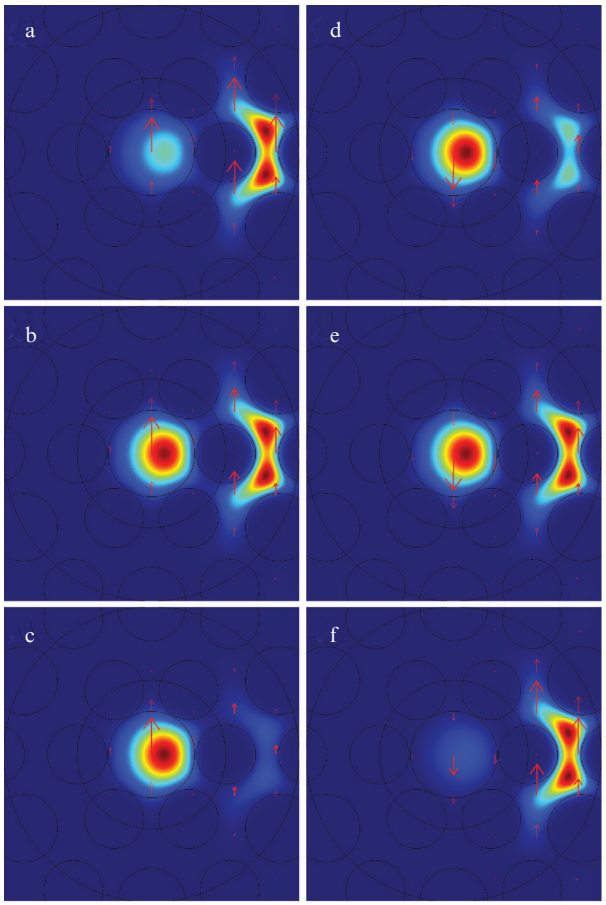

Figure 10. (Colour online) Spatial intensity distributions for modes (a–c) 1a and (d–f) 1b in a bent MOF-18 at $R_x = 0.08$ m for wavelength of (a, d) 0.8050, (b, e) 0.8075, and (c, f) 0.8150 μm.

Figure 11 shows the spectral dependences of leakage losses for modes 1a and 1b in the wavelength range 0.771–0.849 μm. The character of these dependences well agrees with variations in the intensities of the main and additional maxima of modes 1a and 1b in the annular space as shown in Fig. 10. With decreasing wavelength, the integral fraction of the intensity of mode 1a increases in the annular space located rather close to the outer boundary of the cladding, which leads to an increase in the mode leakage losses. On the contrary, an increase in leakage losses for mode 1b occurs with increasing wavelength and is also related to increasing integral fraction of the mode intensity in the annular space. The resultant spectral dependence of leakage losses for mode 1 in this range (see Fig. 7a) corresponds to the minimum among the curves for modes 1a and 1b shown in Fig. 11. A similar situation is observed for mode 2, as well as for modes 1 and 2 in the case of bending in the y direction (Fig. 7b), with slight differences in the positions and heights of peaks.

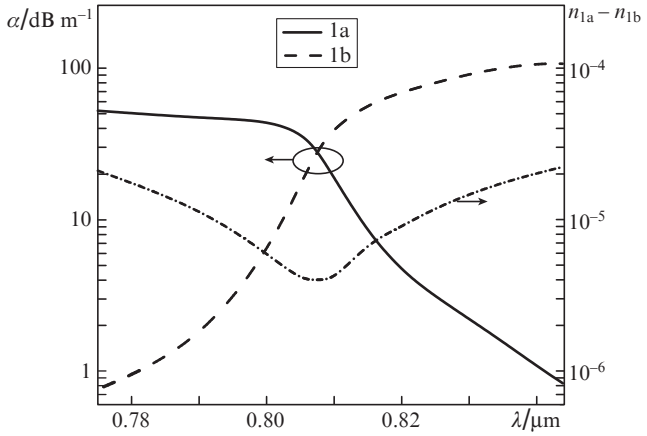

Figure 11. Spectral dependences of leakage losses in a bent MOF-18 at $R_x = 0.08$ m for modes 1a and 1b in the range 0.771–0.849 μm, as well as difference between effective refractive indices n_{1a}–n_{1b} for these modes.

Figure 11 also presents the spectral dependence of the difference between the effective refractive indices of modes 1a and 1b $n_{1a} - n_{1b}$ in the wavelength range 0.771–0.849 μm, which shows that this difference is approximately 4×10^{-6} in the range centre and exceeds 2×10^{-5} at the range edges. It is important to note that the effective refractive index is always higher for mode 1a than for mode 1b. The observed difference in the effective refractive indices $n_{1a} - n_{1b}$ can be qualitatively explained using the Kramers–Kronig relations, which reflect the causality principle and, in the particular case, indicate that the existence of absorption (loss) at some wavelength leads to a non-unity refractive index and vice versa. The Kramers–Kronig relations for effective refractive indices of modes in optical fibres were derived in [35], which showed that, if the dispersion and absorption of a material in a spectral range of interest can be neglected, then the propagation (leakage) loss appears in these relations as an effective loss term. Thus, we can suggest that changes in the leakage loss lead to corresponding variations in refractive indices. Since the spectral dependences of leakage losses for modes 1a and 1b (Fig. 11) have opposite characters, the real parts of refractive indices n_{1a} and n_{1b} deviate in opposite directions. As a result, the curve for the difference $n_{1a} - n_{1b}$ has the shape shown in Fig. 11.

Since all these changes occur in a narrow spectral range, they can be in general conventionally described as quasi-resonance transformation (with decreasing wavelength) of the fundamental mode 1a of the core into a cladding mode and simultaneous transformation of cladding mode 1b into the fundamental mode of the core. A similar situation was previously described by us in [36], but there we considered a MOF-30 with air holes and quasi-resonance transformation of higher-order core modes Ma (M = 3–6) into cladding modes and simultaneous transformation of cladding modes

Mb into higher-order core modes. In our case, the higher-order core modes of MOF-18 have at least pairs of close modes Ma and Mb (M = 3–6) for both straight and bent waveguides. Although these pairs have somewhat different leakage losses, they are observed together almost in the entire studied spectral range. Thus, the higher-order modes in MOF-18 are at least doubly degenerate due to the existence of additional different intensity maxima in the annular space. This distinction from MOF-30 is explained by a considerably lower contrast of refractive indices of the basic MOF-18 material (pure silica glass) and the material of the elements of its cladding (fluorine-doped silica glass), which was chosen to be $\Delta n = 4 \times 10^{-3}$, than this contrast for MOF-30 with air holes in the cladding, which was approximately two-orders of magnitude higher.

Concerning some MOF-18 parameters important from the viewpoint of its applications, note again that, in practice, it is impossible to strictly control the orientation of the internal MOF structure with respect to the bend direction, because of which it is desirable to know parameters averaged over different bend directions. Accurate calculation of these averaged parameters is rather laborious, because of which we will try to estimate them approximately. As was noted above, the spectral ranges of the single-mode regime for MOF-18 bent in the directions of the x and y axes almost coincide and the leakage losses for fundamental mode 1 at a wavelength of 1.05 μm are also rather close for bends in different directions. Therefore, we can use as an estimate the arithmetic mean of the spectral dependences of leakage losses for different bend directions (for unpolarised radiation, they also should be averaged by polarisations, that is, by modes 1 and 2). The resulting spectral dependence of the leakage losses in MOF-18 for the fundamental mode at a bending radius of 0.08 m obtained from the data of Fig. 7 is given in Fig. 12. For higher-order modes, we are most interested in knowing their minimum losses, because of which we first determined from the data given in Fig. 7 the minimum leakage losses among all higher modes 3–6 and then found their arithmetical mean over two bending directions (Fig. 12).

Figure 12 shows that the spectral range of the single-mode regime for a bent MOF-18 with a bending radius of 0.08 μm is 0.93–1.26 μm and the leakage losses for the fundamental mode at a wavelength of 1.05 μm are 0.046 dB m^{-1}. As a result, taking into account the parameters for a straight MOF-18, the single-mode range is 0.98–1.26 μm. From Fig. 12, it is also possible to estimate that the ratio of leakage losses for the higher-order modes to that for the fundamental mode exceeds two orders of magnitude in the range of 1.00–1.65 μm and is higher than 200 in the range of 1.05–1.65 μm.

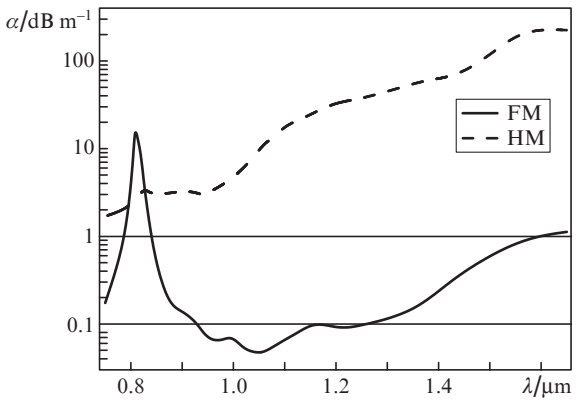

Figure 12. Spectral dependences of leakage losses in a MOF-18 for the fundamental (FM) and higher-order (HM) modes at a bending radius of 0.08 m averaged over bend directions.

One more important parameter of MOF-18 is the dependence of its leakage losses on the bending radius. Figure 13 presents the dependence of leakage losses for the fundamental mode of MOF-18 at a wavelength of 1.05 μm on the bending radius varying in the range 10–4 cm, which is averaged according to the method described above. Note that the losses relatively smoothly increase as the bending radius decrease from 10 to 7 cm, but then sharply increase and reach a maximum near 6 cm, after which decrease. This character (with very slight variations) is observed for modes 1 and 2 for bending in directions of both the x and y axes, which once again demonstrates the important MOF-18 feature consisting in relative independence of its parameters from the bending direction.

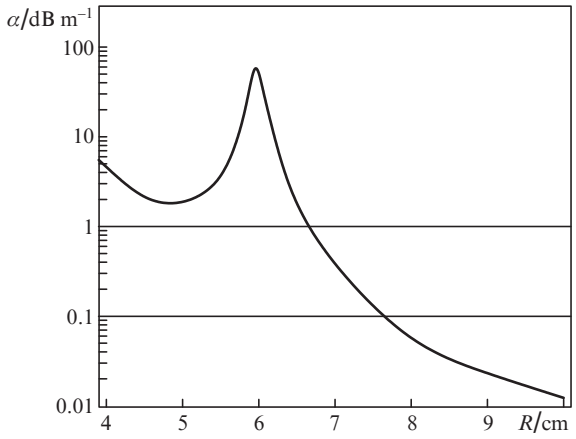

Figure 13. Dependence of leakage losses in a MOF-18 for a wavelength of 1.05 μm on the bending radius averaged over bend directions.

The physical mechanism of this increase in losses at a bending radius of about 6 cm is caused by the existence of modes 1a and 1b, as well as 2a and 2b, which have similar intensity distributions in the MOF-18 core but also have additional intensity maxima in the annular space, that is, in the cladding region. Therefore, we observe the same situation as in the case of a bending radius of 8 cm for a wavelength near 0.8 μm (Fig. 7). Figure 14 shows the spatial intensity distributions of modes 1a and 1b of a MOF-18 bent in the x axis direction at a wavelength of 1.05 μm for bending radii of 5.85, 5.95, and 6.05 cm. Comparison of Fig. 14 with Fig 10 allows us to unambiguously conclude that the physical mechanism is the same in both cases, that is, in the case of Fig. 10 (near a wavelength of 0.8 μm for a bending radius of 8 cm), a decrease in the wavelength is accompanied by quasi-resonance transformation of the fundamental core modes 1a and 2a into cladding modes and simultaneous transformation of cladding modes 1b and 2b into the fundamental modes of the core, and, in the case of Fig. 14 (near a bending radius of 6 cm at a wavelength of 1.05 μm), the same transformations occur with decreasing bending radius.

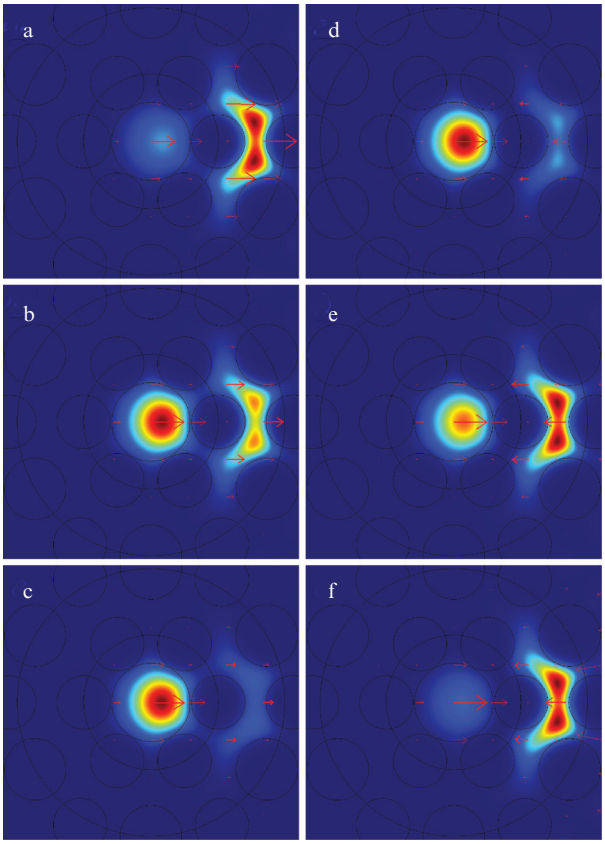

Figure 14. (Colour online) Spatial intensity distributions of modes (a–c) 1a and (d–f) 1b in a MOF-18 bent in the x axis direction at a wavelength of 1.05 μm for bending radii of (a, d) 5.85, (b, e) 5.95, and (c, f) 6.05 cm.

Although such a rapid growth of bend loss may be undesirable, it can be easily eliminated if necessary. Our analysis performed in [36] showed that the positions of these maxima depend on the width of the annular space, because of which one should simply select appropriate MOF-18 parameters for a particular problem.

5. Conclusions

We performed detailed theoretical investigations of the characteristics of original all-glass microstructured optical fibres MOF-18. The leakage losses for the fundamental and four main higher-order modes in the spectral range 0.75–1.65 μm are calculated for MOF-18, both straight and bent with a bending radius of 0.08 m in two orthogonal directions. It is shown that higher-order modes for MOF-18 are at least doubly degenerate due to the presence of different additional intensity maxima in the annular space for both straight and bent waveguides. It is noted that, at the chosen parameters of the structure, MOF-18 have a rather close characteristics at bending in different directions, which is important for practical applications. It is also shown that MOF-18 with these parameters can operate in a single-mode regime in the spectral range 0.98–1.26 μm at a bending radius of down to 0.08 m, the leakage losses for bent MOF-18 at a wavelength of 1.05 μm being 0.046 dB m^{-1}.

Acknowledgements. This work was supported by the Center of Excellence "Center of Photonics" funded by the Ministry of Science and Higher Education of the Russian Federation under Contract 075-15-2020-912.

References

1. Kong F., Gu G., Hawkins T.W., Jones M., Parsons J., Kalichevsky-Dong M.T., Pulford B., Dajani I., Dong L. *Frontiers in Optics 2016. OSA Techn. Digest (online)* (Optical Society of America, 2016) paper FW5B.3.
2. Matniyaz T., Kalichevsky-Dong M.T., Hawkins T.W., Parsons J., Gu G., Li W., Faykus M., Selee B., Dong J.A., Dong L. *Laser Congress 2018 (ASSL), OSA Techn. Digest* (Optical Society of America, 2018) paper AM6A.28.
3. Wang M., Wang F., Feng S., Yu C., Wang S., Zhou Q., Zhang L., Lou F., Chen D., Hu L. *Chin. Opt. Lett*., **17**, 071401 (2019).
4. Pierron R., Chabrol G., Roques S., Pfeiffer P., Yehouessi J.-P., Bouwmans G., Lecler S. *Opt. Lett*., **44**, 2474 (2019).
5. Matniyaz T., Kong F., Kalichevsky-Dong M.T., Dong L. *Opt. Lett*., **45**, 2910 (2020).
6. Egorova O.N., Semjonov S.L., Kosolapov A.F., Denisov A.N., Pryamikov A.D., Gaponov D.A., Biriukov A.S., Dianov E.M., Salganskii M.Y., Khopin V.F., Yashkov M.V., Gurianov A.N., Kuksenkov D.V. *Opt. Express*, **16**, 11735 (2008).
7. Egorova O.N., Semjonov S.L., Vel'miskin V.V., Salganskii M.Yu., Yashkov M.V., Gur'yanov A.N., Dianov E.M. *Quantum Electron*., **40**, 1137 (2010) [*Kvantovaya Elektron*., **40**, 1137 (2010)].
8. Kashiwagi M., Saitoh K., Takenaga K., Tanigawa S., Matsuo S., Fujimaki M. *Opt. Lett*., **37**, 1292 (2012).
9. Kashiwagi M., Saitoh K., Takenaga K., Tanigawa S., Matsuo S., Fujimaki M. *Opt. Express*, **20**, 15061 (2012).
10. Saitoh S., Saitoh K., Kashiwagi M., Matsuo S., Dong L. *J. Lightwave Technol*., **32**, 440 (2014).
11. Gu G., Kong F., Hawkins T., Parsons J., Jones M., Dunn C., Kalichevsky-Dong M.T., Saitoh K., Dong L. *Opt. Express*, **22**, 13962 (2014).
12. Kong F., Gu G., Hawkins T.W., Jones M., Parsons J., Kalichevsky-Dong M.T., Palese S.P., Cheung E., Dong L. *Opt. Express*, **26**, 3138 (2018).
13. Matniyaz T., Li W., Kalichevsky-Dong M., Hawkins T.W., Parsons J., Gu G., Dong L. *Opt. Lett*., **44**, 807 (2019).
14. Février S., Jamier R., Blondy J.-M., Semjonov S.L., Likhachev M.E., Bubnov M.M., Dianov E.M., Khopin V.F., Salganskii M.Y., Guryanov A.N. *Opt. Express*, **14**, 562 (2006).
15. Aleshkina S.S., Likhachev M.E., Pryamikov A.D., Gaponov D.A., Denisov A.N., Semjonov S.L., Bubnov M.M., Salganskii M.Yu., Guryanov A.N. *Proc. SPIE*, **7714**, 771413 (2010).
16. Aleshkina S.S., Likhachev M.E., Pryamikov A.D., Gaponov D.A., Denisov A.N., Bubnov M.M., Salganskii M.Yu., Laptev A.Yu., Guryanov A.N., Uspenskii Y.A., Popov N.L., Février S. *Opt. Lett*., **36**, 3566 (2011).
17. Vanvincq O., Habert R., Cassez A., Baudelle K., Labat D., Delobel S., Quiquempois Y., Bouwmans G., Bigot L. *Opt. Lett*., **45**, 1946 (2020).
18. Wong W.S., Peng X., McLaughlin J.M., Dong L. *Opt. Lett*., **30**, 2855 (2005).
19. Dong L., Peng X., Li J. *J. Opt. Soc. Am. B*, **24**, 1689 (2007).
20. Rosa L., Saitoh K., Tsuchida Y., Varshney S.K., Koshiba M., Poli F., Passaro D., Cucinotta A., Selleri S., Vincetti L., in *Integrated Photonics and Nanophotonics Research and Applications* (Optical Society of America, 2008) paper IWB3. DOI: 10.1364/IPNRA.2008.IWB3.
21. Gu G., Kong F., Hawkins T.W., Foy P., Wei K., Samson B., Dong L. *Opt. Express*, **21**, 24039 (2013).
22. Calvet P., Perrin A., Gouriou P., Samson B., Hawkins T.W., Kong F., Dong L., Dupriez P., Hugonnot E. *Advanced Photonics 2014, OSA Techn. Digest (online)* (Optical Society of America, 2014) paper SoM3B.4.
23. Dong L., Li J., McKay H.A., Fu L., Thomas B.K. *Proc. SPIE*, **7195**, 71950N1 (2009).
24. Saitoh K., Tsuchida Y., Rosa L., Koshiba M., Poli F., Cucinotta A., Selleri S., Pal M., Paul M., Ghosh D., Bhadra S. *Opt. Express*, **17**, 4913 (2009).
25. Dong L., Wu T., Mckay H.A., Fu L., Li J., Winful H.G. *IEEE J. Sel. Top. Quantum Electron*., **15**, 47 (2009).

26. Dong L., Mckay H.A., Marcinkevicius A., Fu L., Li J., Thomas B.K., Fermann M.E. *J. Lightwave Technol*., **27**, 1565 (2009).
27. Saitoh K., Varshney S., Sasaki K., Rosa L., Pal M., Paul M.C., Ghosh D., Bhadra S.K., Koshiba M. *J. Lightwave Technol*., **29**, 2609 (2011).
28. Denisov A.N., Semjonov S.L. *Dokl. Phys*., **66**, 64 (2021) [*Dokl. Ross. Akad. Nauk. Fiz. Tekh. Nauki*, **497**, 12 (2021)].
29. Rashidi K., Mirjalili S.M., Taleb H., Fathi D. *J. Lightwave Technol*., **36**, 5626 (2018).
30. Agraval G. *Nonlinear Fiber Optics* (New York: Acad. Press, 1989; Moscow: Mir, 1996).
31. Guobin R., Zhi W., Shuqin L., Shuisheng J. *Opt. Express*, **11**, 1310 (2003).
32. Kuhlmey B.T., McPhedran R.C., de Sterke C.M. *Opt. Lett*., **27**, 1684 (2002).
33. Tsuchida Y., Saitoh K., Koshiba M. *Opt. Express*, **13**, 4770 (2005).
34. Schermer R.T. *Opt. Express*, **15**, 15674 (2007).
35. Haakestad M.W., Skaar J. *Opt. Express*, **13**, 9922 (2005).
36. Denisov A.N., Semjonov S.L. *Quantum Electron*., **51**, 240 (2021) [*Kvantovaya Elektron*., **51**, 240 (2021)].